Dalton Transactions

ROYAL SOCIETY OF CHEMISTRY

PAPER

View Article Online
View Journal

Cite this: DOI: 10.1039/d2dt02195a

Tunable physics through coordination chemistry: formation on oxide surface of Ti and Al chelates with 3-hydroxyflavone capable of electron injection and light emission†

Getachew Solomon, [a] Anton Landström,[a] Silvia Rotta Loria,[b] Eleonora Bolli,[e] Alberto Mezzetti,[f] Anna Facibeni, [c,d] Sandro Cattarin, [g] Alessio Mezzi,[e] Stefano Protti, [h] Saulius Kaciulis, [e] Margherita Zavelani-Rossi [c,d] and Isabella Concina *[a]

The optoelectronic features of 3-hydroxyflavone (3HF) self-assembled on the surface of an n-type semiconducting metal oxide (TiO_2) and an insulator (Al_2O_3) are herein investigated. 3HF molecules use the coordinatively unsaturated metal ions present on the oxide surface to form metal complexes, which exhibit different behaviors upon light irradiation, depending on the nature of the metal ion. Specifically, we show that the photoluminescence of the surface species can be modulated according to the chemical properties of the complex (*i.e.* the binding metal ion), resulting in solid-state emitters in a high quantum yield (about 15%). Furthermore, photoinduced charge injection can be promoted or inhibited, providing a multifunctional hybrid system.

Received 8th July 2022,
Accepted 1st November 2022
DOI: 10.1039/d2dt02195a
rsc.li/dalton

Introduction

Flavonoids (FLAs) are organic molecules that find multifaceted applications, including as antioxidant,[1] neuroprotective[2] and anti-cancer molecules,[3] and analytical reagents, among others.[4] The FLA core consists of two aromatic rings connected by a pyrane moiety (shown in Fig. 1); interestingly, such a skeleton can be functionalized with different groups, imparting specific photophysical characteristics to the molecules. In particular, flavonols contain an –OH group at the 3-position, and the simplest molecule belonging to this class, 3-hydroxyflavone (3HF), is used as a model in the investigation of the photophysics of such derivatives. Indeed, the emission properties of 3HF strictly depend on the surrounding microenvironment, which can favor different phenomena, including excited state intramolecular proton transfer (ESIPT) and ground state proton transfer, thus resulting in a double or even a triple emission profile.[5,6]

Whereas the photophysics of 3HF has been deeply investigated in solution,[5] little information is available about its behavior in solid matrices[6–8] and its combination with inorganic,

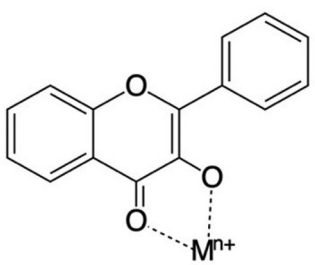

Fig. 1 3-Hydroxyflavone (3HF) chemical structure, also showing the binding site in the formation of metal complexes (the IUPAC numbering is shown in blue).

[a]*Department of Engineering Sciences and Mathematics, Luleå University of Technology, 97187 Luleå, Sweden. E-mail: isabella.concina@ltu.se*
[b]*Dipartimento di Fisica, Politecnico di Milano, piazza L. da Vinci 32, 20133 Milano, Italy*
[c]*Dipartimento di Energia, Politecnico di Milano, via G. Ponzio 34/3, 20133 Milano, Italy*
[d]*IFN-CNR, piazza L. da Vinci 32, 20133 Milano, Italy*
[e]*Institute for the Study of Nanostructured Materials, ISMN-CNR, 00015 Monterotondo Stazione, Roma, Italy*
[f]*Laboratoire de Réactivité de Surface (LRS), Sorbonne Université, CNRS, 4 Place Jussieu, Paris 75005, France*
[g]*Istituto di Chimica della Materia Condensata e di Tecnologie per l'Energia, ICMATE-CNR, C.so Stati Uniti 4, 35127 Padova, Italy*
[h]*Photogreen Lab, Department of Chemistry, University of Pavia, Viale Taramelli 10, 27100 Pavia, Italy*

† Electronic supplementary information (ESI) available: XRD patterns, EDX analysis, kinetics of 3HF uploaded on TiO_2 nanoparticle films, emission of 3HF in solution, XPS and UPS details, details of electrochemistry experiments, pump and probe analysis and setup description are reported in the supporting information. See DOI: https://doi.org/10.1039/d2dt02195a

biocompatible, and nanosized materials, such as metal oxides.[9,10]

Furthermore, the coordination chemistry in the solution of FLAs with different metal ions, like Al^{3+}, Zn^{2+} and Pb^{2+},[11] resulting in the formation of 3HF–metal complexes (Fig. 1 shows the binding site of 3HF), is well known, but a complete characterization of the structure–property relationship is still lacking.[12,13] It is noteworthy that the physics and chemistry of these species, once self-assembled as molecular films on metal oxide, where metal ions constitute thermodynamically favored sites for chelation, have seldom been investigated with a specific focus on the effect of chemisorption on the emission properties of FLAs. Indeed, a literature search only results in a few studies on their specific use as photosensitizers, especially in solar cells[14–19] and photocatalysts,[20] and it has been reported that morin (a 3HF derivative) can bind TiO_2 nanoparticles (NPs).[21,22]

Self-assembled monolayers (SAMs) are spontaneously adsorbed and ordered monolayers of molecules on planar and nonplanar substrates, generating just one molecule thick films. The interest in SAMs emerged with the aim of creating a hetero-interface, whose properties can be finely tuned and whose utility has been demonstrated in a broad range of fields.[23] However, most research carried out focuses on the adsorption of medium- to long-chain organic molecules (especially alkanethiols, silanes and phosphonic acids) on gold, while very little can be found concerning the use of metal oxide surfaces, although they are known to be suitable as anchoring sites for a variety of organic molecules, and given that these latter possess proper functional groups enabling physisorption or chemisorption.[24]

Deposition of thin layers of metal oxides *via* atomic layer deposition (ALD) is a well-established strategy to impact the charge transport between the underlying material and the surroundings.[25] It has been applied in dye-sensitized solar cells to investigate its effect on charge injection and recombination[26,27] and dye photostability.[28,29]

In the present study, we investigated the photophysics of 3HF chemisorbed on TiO_2 NPs, with and without a conformal Al_2O_3 layer of variable thickness (30 and 100 Å). Fast uptake kinetics, spurred by the chelation of the surface metal ions, coordinatively unsaturated[30,31] by an organic fluorophore, result in the formation of a surface complex, whose photoluminescence is lowered or enhanced depending on the specific metal ion (Ti^{IV} and Al^{III}). The expected photoinduced charge transfer from the excited 3HF to TiO_2 can be tuned through the modulation of the thickness of the insulating layer, thus supporting or quenching the emission process.

Experimental methods

Sample preparation

Anatase TiO_2 nanoparticle films were prepared *via* tape casting of 18NR-T (20 nm) Dyesol paste on FTO glass (Pilkington TEC 15, 15 Ω sq^{-1}). The Al_2O_3 layer was deposited using a Cambridge NanoTech Savannah 200 atomic layer deposition system. Highly pure nitrogen (99.999%) was used as both the carrier and purging gas. The tri-methyl aluminum (TMA) precursor was used as the aluminum source and ultra-pure H_2O as the oxidation agent. The pulse times for both precursors were 0.015 seconds. Application of these parameters resulted in a growth rate of 1 Å per cycle (according to the Sigma Aldrich ALD chemical suppliers). For 100 ALD cycles, nearly 10 nm thickness of Al_2O_3 was obtained.[32] The deposition temperature was maintained at 150 °C without heating the precursors. The Al_2O_3 thickness was controlled by adjusting the number of ALD cycles.

The insulating Al_2O_3 layers on top of TiO_2 (samples labelled as Al_2O_3–TiO_2) featured nominal thicknesses of approximately 30 Å and100 Å, respectively.

The adsorption of 3HF onto the films was performed by preparing a 10^{-3} M solution of 3HF in ethanol (95%), then soaking the films. The nominal pH of the solutions was modulated by adding either hydrochloric acid or potassium acetate, to force the 3HF molecules into their protonated or unprotonated forms (nominal pH: 4 and 8, respectively).

3-Hydroxyflavone (3HF) was purchased from TCI Chemicals and re-crystallized using cyclohexane before use. Ti(*n*BuO)$_4$ and Al(iPrO)$_3$ were used for the formation of the corresponding 3HF–metal complexes. A 50 μM solution of 3HF in MeOH was used in all the experiments. The formation of the Al- and Ti-based complexes was achieved using Al(iPrO)$_3$ and Ti(*n*BuO)$_4$, respectively. An excess of metal ions (3 equiv. for Al(III) and 5 equiv. for Ti(IV)) was used in order to achieve the quantitative formation of the complex.

Characterization

An Agilent Cary5000 spectrophotometer was used to record transmittance/absorbance spectra. The emission spectra of 3HF anchored on the metal oxides were recorded on an Edinburgh Instruments FLS980 spectrofluorometer on the films after drying them in air. The absolute photoluminescence quantum yield (QY) of 3HF anchored on metal oxide films was measured using an integrating sphere. The fluorescence spectra of 3HF– and 3HF–metal complexes in solution were recorded on a PerkinElmer LS55 spectrofluorometer. IR absorption spectra were recorded on a Bruker Hyperion 2000 microscope with an LN-cooled MCT detector and an ATR objective. For obtaining the spectra of uncoordinated 3HF, 3HF was mixed with KBr and measured in reflectance mode with the Schwarzschild objective. The spectra were recorded with a resolution of 4 cm^{-1}.

The photocurrent response and electrochemical impedance spectroscopy (EIS) were performed in a common three-electrode configuration using a ModuLab XM ECS Potentiostat (Solartron Instrument). An Ag/AgCl electrode and a Pt plate were used as the reference and counter electrodes, respectively. The as-prepared samples on fluorine-doped tin oxide glass (0.8 × 0.8 cm^2 active area) were directly used as a working electrode. All (photo)electrochemical measurements were performed in an electrolyte solution of 0.1 M Na_2SO_4 + 0.2 M LiI at different values of pH. The working solutions were deoxygenated by

purging them with purified argon gas (99.999%) for 10 min before electrochemical experiments. The samples were illuminated in pulse mode (on/off) using a Thorlabs C2200 Touchscreen LED system under UV and white light illumination sources, separately. EIS spectra were measured at 0.3 V *vs.* Ag/AgCl over the frequency spectrum range from 100 kHz to 50 mHz at an AC amplitude of 5 mV. EIS data were fitted using commercial software (RelaxIS impedance analysis software).

X-ray photoelectron spectroscopy (XPS) analyses were carried out using an electronic spectrometer Escalab 250Xi (Thermo Fisher Scientific Ltd, UK). The oxide films before and after the adsorption of 3HF were introduced into the analysis chamber, where the base pressure was maintained at $\sim 2 \times 10^{-9}$ mbar. The reference sample of 3HF powder was mounted on grated pure Au foil (99.99%). The photoemission spectra were excited with a monochromatized Al Kα source and registered using a 6-channeltron detection system at a constant pass energy of 40 eV. The binding energy (BE) scale was calibrated by setting the aliphatic carbon peak C 1s at BE = 285.0 eV. The electromagnetic input lens was set to standard mode with a diameter of about 1 mm of the analyzed area. To eliminate the sample charging under X-rays, two low-energy (1 eV) flood sources were used: an in-lens electron beam and an external Ar^+ ion beam. All experimental data were acquired and processed using the Avantage v.5 software (Thermo Fisher Scientific Ltd, UK). The "smart" background and mixed Lorentzian/Gaussian peak shape were used for the peak fitting routine. Scofield's relative sensitive factors with the energy compensation coefficient of $KE^{0.6}$ were applied for the elemental quantification.

The pump–probe setup was based on a commercial amplified Ti:Sapphire laser system (Coherent Libra-HE) delivering about 100 fs pulses at a 2 kHz repetition rate with a central wavelength of 800 nm. The pump beam at 400 nm was obtained by frequency doubling in a 1 mm thick β-barium borate crystal and was propagated through a mechanical chopper running at 1 kHz. As a probe pulse, a white light continuum generated in a 3 mm-thick CaF_2 plate was employed. An optical multichannel analyser then recorded the differential transmission of the probe beam both when the chopper blocked the pump or not. The transient transmission was then computed using $\Delta T/T = (T_{ON} - T_{OFF})/T_{OFF}$ for all wavelengths of the white light continuum as a function of the pump–probe time delay. As the pump fluence, for the sake of comparison, the amount of energy impinging on the TiO_2 NP film was considered, after transmission through the 3HF film, so as to directly access the contribution to the signal arising from TiO_2 and 3HF. The measurements were performed at an ambient temperature.

Results and discussion

Commercial TiO_2 nanoparticles (NPs) were used to deposit a film (about 3 μm thick) on standard conductive glass, followed by their coverage with an Al_2O_3 layer, whose thickness was tuned during the generation through atomic layer deposition (ALD). The as-prepared oxides were characterized by X-ray diffraction (XRD) and energy dispersive X-ray spectroscopy (EDX) (the analyses are shown in Fig. S1 and Fig. S2, respectively, in the ESI†). The ALD deposition parameters were adjusted to produce two sets of samples, featuring different Al_2O_3 thicknesses (30 Å and 100 Å).[32] The absence of a crystalline pattern in the alumina layer (Fig. S1 in the ESI†) is an indirect confirmation of the very small thickness of the insulating layer, while its presence is confirmed by the EDX mapping, which shows a conformal coverage of the underlying semiconductor within a micrometric resolution (Fig. S2 in the ESI†) and elemental analysis (Table S1 in the ESI†). Furthermore, the presence of Al_2O_3 on the TiO_2 surface was also shown by XPS analysis, discussed in detail below.

After the film preparation, the samples were soaked in a 3HF ethanolic solution and the evolution of their optical feature was characterized by means of spectrophotometry and photoluminescence.

Fig. 2a shows the absorption spectra of 3HF in ethanol at different nominal pH: while the overall spectrum was almost unchanged upon pH variation, a new spectral feature emerged as an unresolved band around 415 nm at basic pH and a low, weak shoulder band in the case of neutral ethanol. In accordance with the available literature,[33] the absorption band at 415 nm was assigned to the anionic form of 3HF.[33]

Before investigating the binding mode of 3HF on a metal oxide surface, we analyzed the adsorption kinetics by means of spectrophotometry. For this purpose, a TiO_2 nanoparticle (NP) film was used as a model: the film was soaked in a 3HF ethanolic solution for increasing soaking times and the evolution of the spectral feature was then analyzed. Fig. 2b reports the absorption spectra of 3HF loaded onto the TiO_2 NPs, at nominal pH 4 (black lines) and 8 (blue lines). The presence of 3HF on the NP surface induced the appearance of a shoulder band at around 415 nm (irrespective of the pH of the soaking solution), whose intensity steadily increased at increasing soaking times (see Fig. S3a in the ESI†). The analysis over the time of the absorption intensity at 415 nm (reported in Fig. S3b in the ESI†) showed that the kinetics of adsorption consists of two contributions, which are well fitted by an exponential curve and a straight line, according to the model reported in the ESI (eqn (1)–(5)).† This 2-step kinetics was expected and we have previously investigated the dynamics of the uploading of a dye on the TiO_2 surface, to enable a rational control of the amount of loaded organics,[34] which plays a critical role in certain applications.

The present case, however, revealed a different behavior: on the one hand, the system reached saturation in a very short time (in about 15 min) compared to that observed in similar studies, analyzing the kinetics of uptaking organic molecules on metal oxide surfaces.[34] Furthermore, the observed kinetics was independent of the nominal pH of the original 3HF solution, which also showed no influence on the spectral features of the 3HF-loaded metal oxide films (Fig. 2b). Moreover, the amount of 3HF anchored on the metal oxide surface was quite

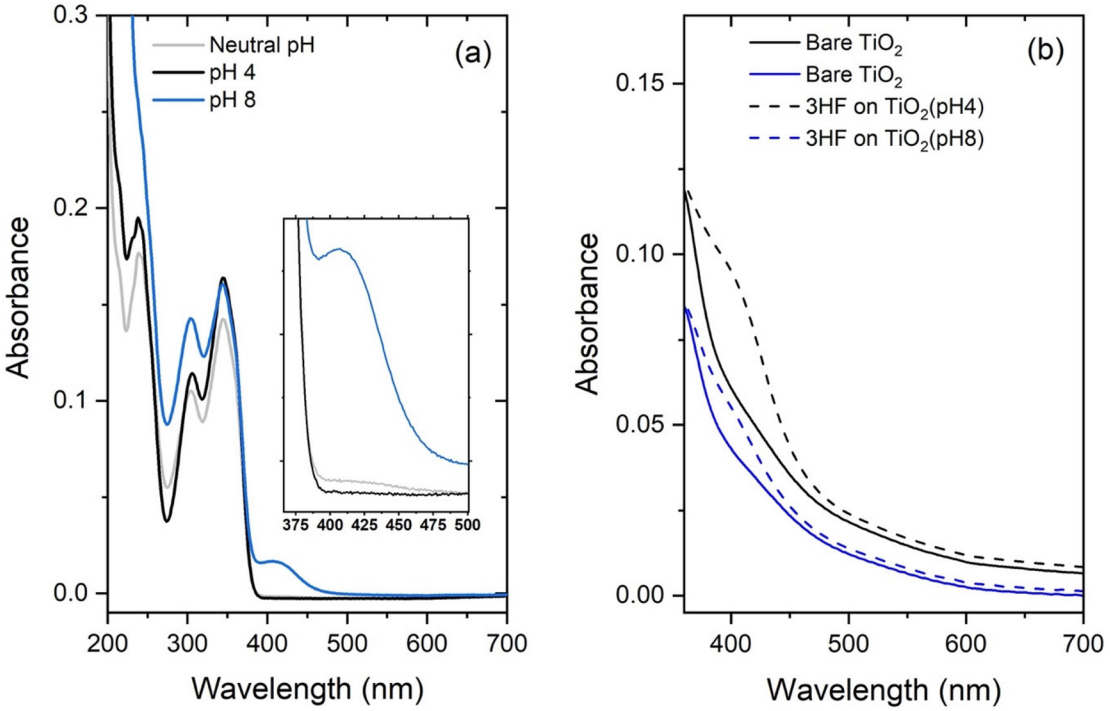

Fig. 2 (a) Absorption spectra of 3-hydroxyflavone (3HF) in acidic (black line, nominal pH = 4), neutral (grey line), and basic (blue line, nominal pH = 8) solution in ethanol. The inset shows the detail of the 350–550 nm region, highlighting the presence of a band ascribable to the 3HF anion in the case of basic pH (slightly hinted also in neutral pH). (b) Absorption spectra of bare transparent TiO_2 before (dashed lines) and after 3HF uptake (solid lines). Black line: soaking at nominal pH 4; blue line: soaking at nominal pH 8.

low, and we will better show a detailed analysis of the surface composition through X-ray photoelectron spectroscopy. These observations suggest the presence of a strong driving force spurring 3HF anchoring on the TiO_2 surface and at the same time indicate that: (i) the number of available sites for binding is limited and (ii) there was no formation of 3HF multilayers on the metal oxide surface, due to aggregation phenomena (as previously reported for other molecules used as dyes).[35]

Dual emission bands (centered at 401 nm and 531 nm) were observed for 3HF in several alcohols used as solvent[36] (see Fig. S4 in the ESI†). As broadly reported in the literature, the absorption of UV light leads to the excitation of 3HF from the enol ground state N to the singlet N* excited state.[37,38] The excitation is then followed by ESIPT from 3-OH to the C=O group, to give the tautomeric excited form T*, emitting in the 500–540 nm region.[36,37] It should be remembered that, in polar or protic media, the ESIPT is hindered, and the radiative decay from N* to N states is more favored, compared to apolar media. The spectral characteristics are thus strictly dependent on the surrounding environments.

The emission spectrum of 3HF in ethanol (Fig. S4 in the ESI†) is not dependent on the pH of the solution, thus showing that the hydrogen of the 3-OH group is present in all cases, and is still participating in the emission processes. Anchoring on the surface of a metal oxide, both titanium dioxide and alumina resulted instead in a change in the emission features (Fig. 3a and b). Fluorescence emission of 3HF bound to TiO_2 consists of a single peak, centered at about 460 nm (FWHM = 60 nm), featuring a weak intensity, especially when the metal oxide is soaked in the lower pH solution. Furthermore, the observed emission wavelength does not match the emission of the deprotonated molecule.[37] The deposition of the Al_2O_3 layer on TiO_2 NPs and the subsequent anchoring of 3HF resulted in an intense photoluminescence emission, also centered at 460 nm (FWHM = 60 nm). Quantification of the quantum yield (QY) in this latter case showed a value as high as 15.3% ± 0.8 for an Al_2O_3 thickness of 100 Å, and 14.2% ± 0.7 for an Al_2O_3 thickness of 30 Å. The results point out that more physisorption is occurring in the materials under investigation and that a process in competition with the decay through light emission takes place in all the systems.

In order to understand these experimental observations, we adopted a multi-technique analytical approach: we characterized the fluorophore–metal oxide samples by means of Fourier transform infrared (FTIR) spectroscopy to investigate the bonds formed between the 3HF and the metal oxides (results are shown in Fig. 4), while at the same time analyzing their surfaces by means of X-ray photoemission spectroscopy (XPS) (shown in Fig. 5–7, Tables 1, 2, Fig. S5, S6 and Tables S2, S3 in the ESI†), to determine the species present on the surface.

TiO_2 NPs without and with a 100 Å Al_2O_3 layer before and after 3HF uptake were thus analyzed by means of FTIR (Fig. 4)

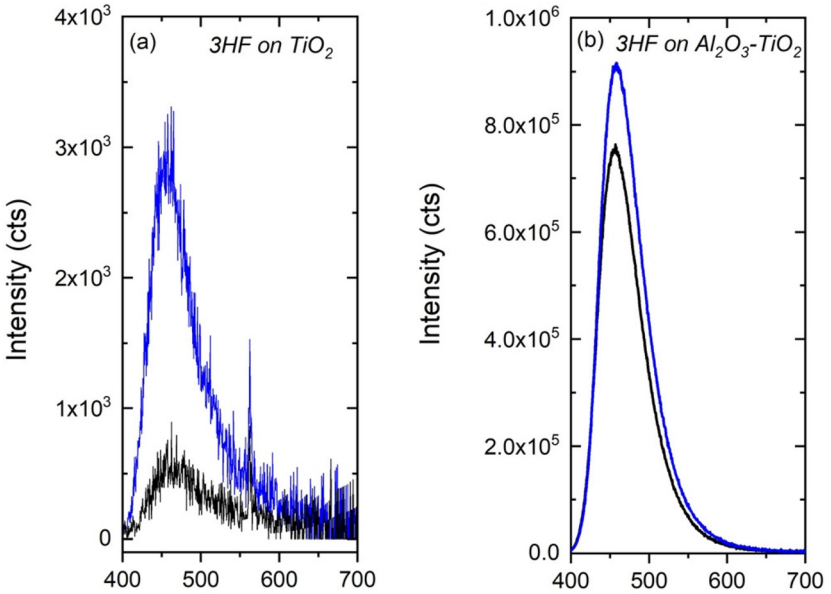

Fig. 3 PL emission features of (a) 3HF on TiO_2, (b) 3HF on Al_2O_3–TiO_2 (100 Å, similar results were obtained for the 30 Å Al_2O_3–TiO_2 sample, data not shown). Black line: soaking at nominal pH 4; blue line: soaking at nominal pH 8. Excitation wavelength: 380 nm.

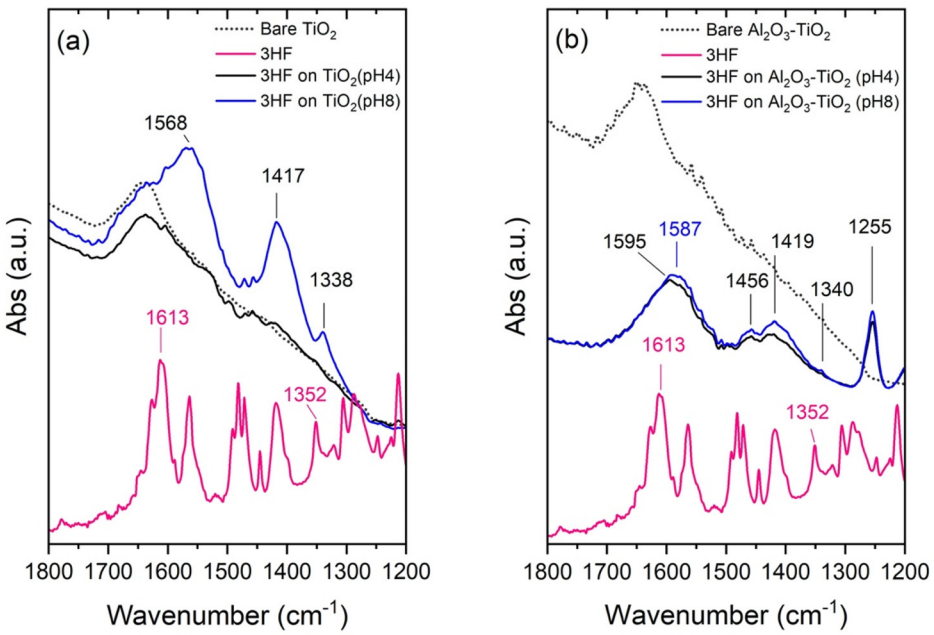

Fig. 4 FTIR spectra of TiO_2 NP film (a) and Al_2O_3–TiO_2 100 Å (b) before (dotted gray lines) and after (solid black and blue lines) the anchoring of 3HF. Solid blue and black lines refer to the uptake at pH 8 and pH 4, respectively. The FTIR spectrum of 3HF (pink line) is reported for comparison purposes.

and the vibrational bands were compared with the IR spectrum of 3HF (similar results were obtained for the thinner Al_2O_3 layer, data not shown). The vibration centered at 1613 cm^{-1} is associated with C=C and C=O stretching in 3HF[7,39] and disappears once the molecule is anchored on the metal oxide. A peak centered at 1587 cm^{-1} (sample soaked at pH 8) and at 1595 cm^{-1} (prepared at pH = 4) appeared in the FTIR spectra of 3HF bound to Al_2O_3 (Fig. 4b): this vibration is ascribable to the asymmetric stretching of a C–O group, featuring a partial character of the double bond, linked to the surface of the metal oxide. The vibration centered at 1255 cm^{-1}, visible as a strong peak in the Al_2O_3–TiO_2 sample but partly hidden in the TiO_2 sample due to the signal of the metal oxide, can be tentatively assigned to C–O stretching.

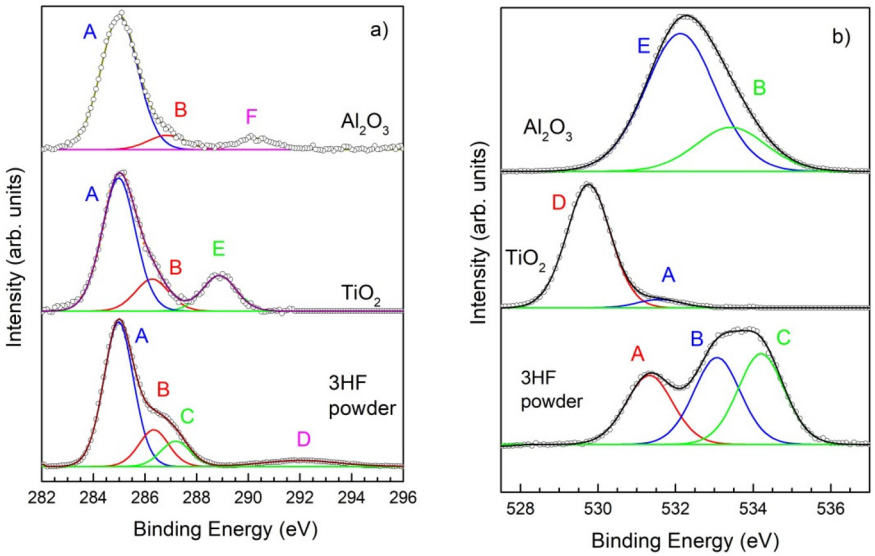

Fig. 5 Comparison of C 1s (a) and O 1s (b) spectra for 3HF reference powder and metal oxides TiO_2 and Al_2O_3–TiO_2.

Table 1 XPS quantification for the Al_2O_3–TiO_2 samples before and after adsorption of 3HF at pH = 8 and pH = 4. The values of Δ are the changes in elemental composition after adsorption; the characteristic fingerprints of 3HF are in bold

Peak	BE, eV	FWHM, eV	at% Al_2O_3	Δ, at% 3HF@pH8	Δ, at% 3HF@pH4	Bond
Al 2p	74.8	1.8	29.7	−1.8	−8.3	Al^{+3}
C 1s – A	284.9	2.0	9.7	+3.4	+0.3	Aliphatic
C 1s – B	286.4	2.0	1.1	**+0.2**	**+2.2**	–C–O
C 1s – C	287.9	2.0	—	—	**+0.6**	C═O
C 1s – F	290.0	2.0	0.9	+0.2	+1.0	Carbonate
O 1s – A	531.0	1.9	—	+16.3	—	$Al(OH)_3$
O 1s – E	532.0	1.9	40.2	−15.6	−19.5	Al_2O_3
O 1s – B	533.1	1.9	12.9	**−3.6**	**+10.6**	C═O
O 1s – C	534.3	1.73	—	—	**+3.0**	–C–O
Si 2p – A	101.8	1.6	3.4	+0.4	−3.4	Al–Si oxide
Si 2p – B	103.2	1.7	1.9	+0.1	−1.9	SiO_2
Ti $2p_{3/2}$	459.3	1.2	0.2	+0.3	+0.3	TiO_2

Table 2 XPS quantification for the TiO_2 samples before and after adsorption of 3HF at pH = 8 and pH = 4. The values of Δ are the changes in elemental composition after adsorption; the characteristic fingerprints of 3HF are in bold

Peak	BE, eV	FWHM, eV	at% TiO_2	Δ, at% 3HF@pH8	Δ, at% 3HF@pH4	Bond
C 1s – A	285.0	1.54	7.5	+1.5	+7.2	Aliphatic
C 1s – B	286.5	1.54	1.8	**−0.4**	**+1.2**	–C–O
C 1s – E	288.4	1.53	4.0	−1.1	−2.1	Carboxyl
O 1s – D	529.7	1.39	57.7	−3.9	−6.7	TiO_2
O 1s – A	531.2	1.39	4.0	**+1.3**	**+1.3**	OH^-
O 1s – B	532.0	1.39	—	**+2.6**	**0**	C═O
Ti 2p	458.4	1.26	27.0	−2.1	−2.9	TiO_2

The chemical composition of the surface of samples before and after the adsorption of 3HF was investigated by XPS. To identify the characteristic photoemission signals, the reference powder of 3HF was also analyzed. As the photoemission signals of 3HF are only those of carbon and oxygen, the spectra of C 1s and O 1s registered for 3HF were compared with the ones for bare films of TiO_2 and Al_2O_3–TiO_2 as shown in Fig. 5.

The elemental quantification of all chemical species of C and O for 3HF reference powder and the quantification for bare substrates are reported in Tables S2, S3 and S4 in the ESI.† The main three components of C 1s and O 1s spectra correspond to the constituent species in the 3HF molecule, and their atomic ratios are also almost stoichiometric: total C : O = 5 and the components of O 1s A : B : C ≈ 1 : 1 : 1 (see Fig. 5 and Table S2†). Therefore, for the identification of 3HF

molecules adsorbed on TiO_2 and Al_2O_3–TiO_2 films, the variation of these species in C 1s and O 1s spectra must be followed. As the first two components (A and B) of C 1s and O 1s in 3HF spectra were overlapping with the components of C 1s and O 1s for the oxide substrates, the most indicative fingerprints of 3HF were the third ones (marked C), attributed to the C═O bond in the C 1s spectra and the –C–O bond in O 1s. In the case of the TiO_2 substrate, the presence of the second component of O 1s (C═O bond) can be monitored as well, as it was absent in the spectrum of bare TiO_2 film.

The photoemission spectra of C 1s and O 1s acquired before and after the treatment of Al_2O_3–TiO_2 film with 3HF at pH = 4 and 8 are presented in Fig. 6.

However, the visual comparison of C 1s and O 1s spectra is hindered by the variation of initial intensity of the main components (A in C 1s and E in O 1s) after treatment with 3HF. For this reason, a more reliable comparison was done from the results of XPS quantification listed in Table 1, in which the changes in elemental composition Δ, *i.e.*, the differences in the atomic concentration before and after the addition of 3HF at nominal pH = 8 and 4, are reported. The highest amount of adsorbed 3HF (the increase in –C–O and C═O components in C 1s and O 1s spectra) was detected in Al_2O_3–TiO_2 film treated at pH = 4.

An analogous comparison of the photoemission spectra of C 1s and O 1s and the quantitative changes Δ for TiO_2 film after treatments with 3HF are presented in Fig. 7 and Table 2, respectively. In TiO_2 film treated at pH = 4, the fingerprints of 3HF were very low: only a slight increase (about 1 at%) of –C–O in the C 1s spectrum (component B) and OH^- in the O 1s spectrum (component A) was observed. From the comparison of 3HF fingerprint variations reported in Tables 1 and 2, it is clear that the adsorption of 3HF on Al_2O_3–TiO_2 film is not visible at pH = 8, whereas in TiO_2, treated at the same pH, a low amount of 3HF is indicated by increased OH^- and C═O (components A and B) in the O 1s spectrum. Therefore, the highest amount of 3HF on Al_2O_3–TiO_2 film was detected at pH = 4 and on TiO_2 film at pH = 8, even if it was significantly lower than that on Al_2O_3–TiO_2 at pH = 4.

The origin of the carbonate component F in Table 1 is due to the initial contamination of bare Al_2O_3–TiO_2 film and 3HF powder (see also Tables S2 and S3 in the ESI†). Therefore, its content is increased after the adsorption of 3HF on the oxide film. The carboxylic component E in Table 2 is already present as the contaminant on the surface of TiO_2 film (see also Table S4 in the ESI†) and decreases after surface coverage with 3HF.

The valence band spectra, acquired with ultraviolet He I (21.2 eV) and II (40.8 eV) sources, did not reveal any noticeable changes after the adsorption of 3HF (see Fig. S5 and S6 in the ESI†). Probably the changes were not visible due to the absence of any characteristic features in the valence band

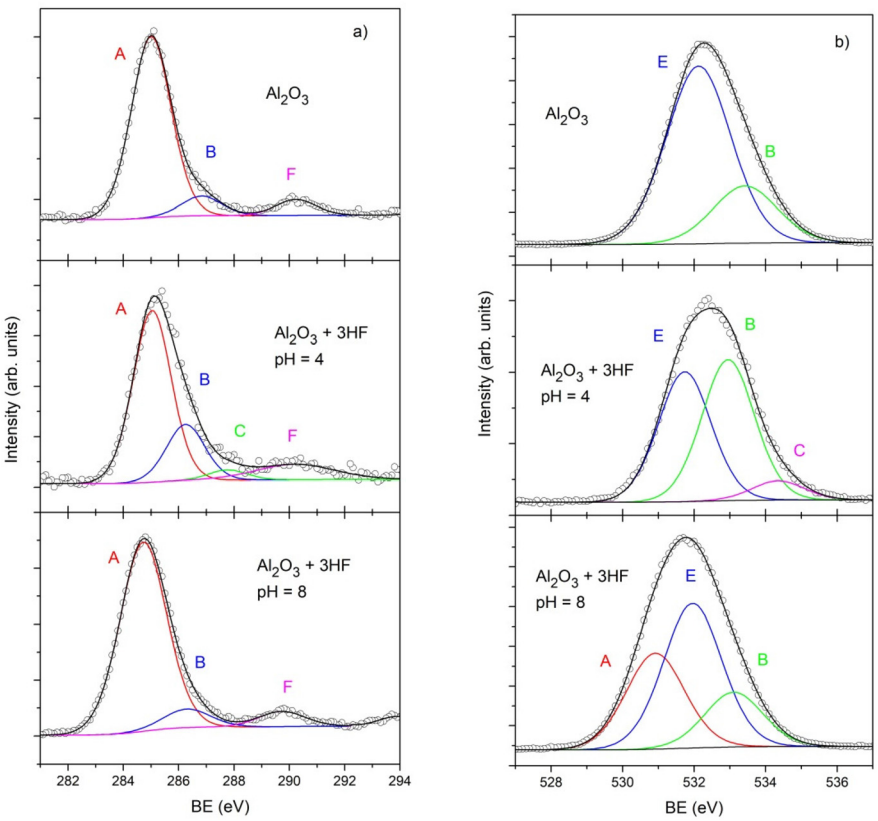

Fig. 6 Comparison of C 1s (a) and O 1s (b) spectra for Al_2O_3–TiO_2 film treated with 3HF at pH = 4 and 8.

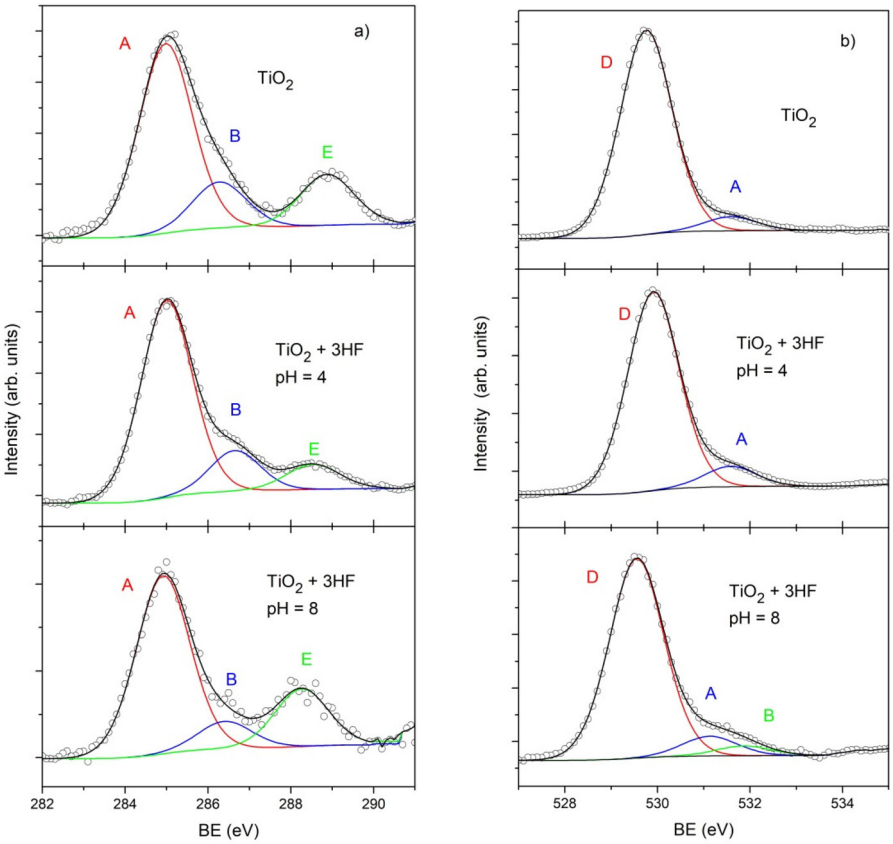

Fig. 7 Comparison of C 1s (a) and O 1s (b) spectra for TiO_2 film treated with 3HF at pH = 4 and 8.

spectra of the 3HF reference sample, whereas in the spectra of both oxides the strong bands of convoluted Ti 3d–O 2p and Al 3p–O 2p levels are present.

Information retrieved from both FTIR and XPS analyses suggests the formation of a surface complex 3HF–M^{n+}. For the sake of comparison, the UV-vis absorption spectra of 3HF in methanol and in the presence of $Ti(OBu)_4$ were recorded, and the results were compared with results available in the literature on the $[Al(3HF)_2]^+$ complex[40,41] This experiment was based on the hypothesis that 3HF can act as a chelating ligand also for metal ions located on the metal oxide surface, as previously suggested for other organic molecules.[42] Fig. 8 shows the electronic absorption and emission spectra recorded in methanol for free 3HF, $[Al(3HF)_2]^+$ complex and 3HF in the presence of a Ti(IV) source ($Ti(n\text{-}OBu)_4$). Analogously to what was observed for $[Al(3HF)_2]^+$, the addition of a Ti(IV) source to a solution of 3HF results in a substantial modification of the UV-absorption profile of the ligand, with a new absorption band located at 402–404 nm. Similar results were obtained by Galland and coworkers, who prepared a $[Ti(3HF)_2]Cl_2$ complex using $TiCl_4$ as a source of the Ti^{IV} core.[43] The emission spectra of the examined species (Fig. 8c–e) further support the formation of the metal–3HF complex. Indeed, when compared to the emission spectra of 3HF in methanol, whose emission band is located at 513 nm (FWHM = 78.3 nm), the photoluminescence features of the Ti^{IV} complex and the Al^{III} complex are very similar: they both show a single peak located at about 467 nm (FWHM = 58 nm), whose intensities are one third less and six orders of magnitude bigger (respectively) than those of bare 3HF in the same solvent, in excellent agreement, for the position and FWHM, with what was observed for the photoluminescence of the fluorophore anchored on the surfaces of TiO_2 and Al_2O_3–TiO_2, respectively (Fig. 3).

This further evidences the formation of surface complexes where the 3HF molecules act as ligands towards the Ti^{IV} and Al^{III} species located on the surface of the metal oxide. The entropy-driven chelate effect was then the driving force spurring the anchoring of 3HF,[23,44–46] also considering that a 5-membered ring is formed upon this bonding mode, which is acknowledged as a particularly stable geometry for organic molecules.[47]

Furthermore, also in solution, a significantly (seven orders of magnitude) weaker photoluminescence emission in the Ti^{IV} complex can be observed, as compared with the high intensity of the signal pertaining to the $[Al(3HF)_2]^+$ species.

In order to gain further information, we carried out two sets of experiments: (i) photocurrent generation to investigate the expected charge injection from the surface complexes in the TiO_2 conduction band (as previously reported in dye-sensitized solar cells using a natural chromophore as light harvesters)[16] and (ii) transient absorption spectroscopy measurements to probe the dynamics of charges photogenerated in

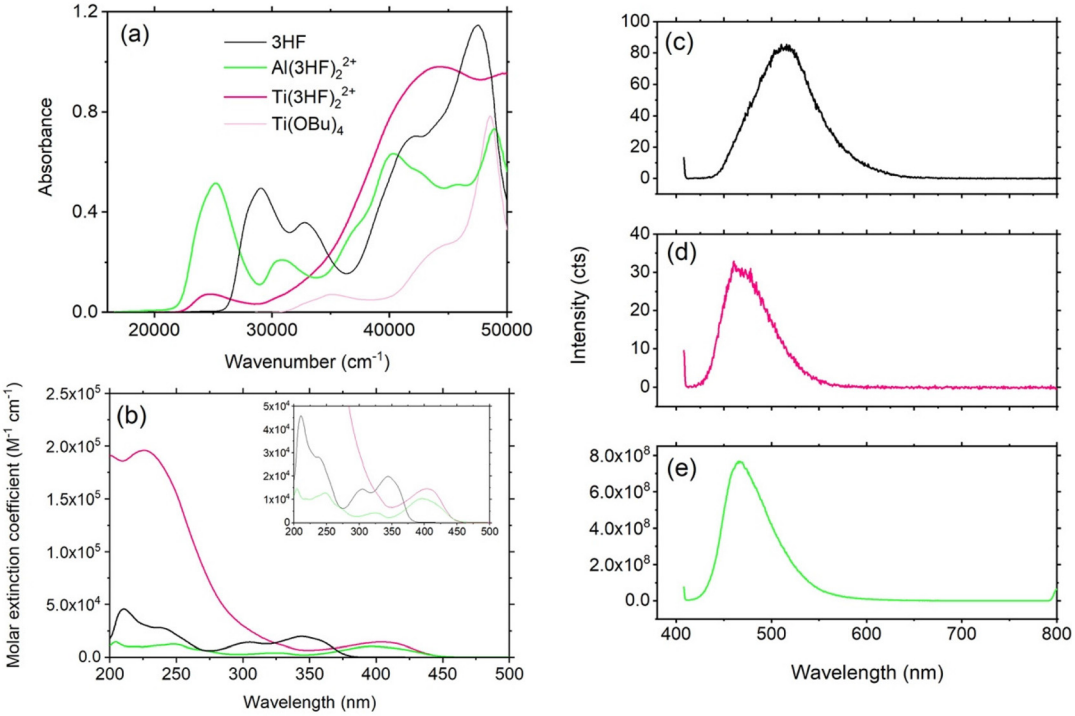

Fig. 8 (a) Electronic absorption spectra, (b) molar extinction coefficient and (c) photoluminescence emission spectra of: 3HF in MeOH (black line); Ti(IV)–3HF complex (pink line); Al(III)–3HF complex (green line). The absorption spectrum of the precursor Ti(*n*-OBu)$_4$ is reported (light pink line) for comparison purposes.

3HF and verify the possibility of their injection into the semiconductor also when covered by a thin insulating layer at a micrometric level.

Investigation of the photoelectrochemical properties was performed in a three-electrode setup, similar to the procedures reported elsewhere[48–50] and described in the experimental part. The light sources used (whose spectra are shown in Fig. S7 in the ESI†) permitted illumination of the electrodes alternately with UV and visible light. Photoaction spectra could not be recorded due to the lack of a monochromator and a phase-sensitive detection system, but the effect of modifications in the spectrum of the incident light was checked using filters.

Fig. S8 in the ESI† shows the photocurrent/potential curves recorded on sweeping the potential from the negative limit in a positive direction while illuminating the electrode with chopped UV light. Both TiO_2 and Al_2O_3–TiO_2 photoelectrodes exhibited anodic photocurrents, increasing progressively with the applied potential. The lower response of Al_2O_3–TiO_2, compared with that of TiO_2, was expected due to the insulation properties of Al_2O_3.

Both TiO_2 and Al_2O_3–TiO_2 bare electrodes appeared almost insensitive to illumination with visible light of wavelength above 400 nm; however, after deposition of a 3HF layer, well-defined and rather stable photocurrent transients were recorded under chopped illumination over an extended potential range (the two recordings are compared in Fig. S9 in the ESI†). This comparison showed that a substantial charge transfer from 3HF to TiO_2 sustains the photocurrent response. According to the mechanism previously suggested,[51] the photogenerated excited molecule injects an electron into the conduction band of the semiconductor, due to favorable energy matching. The resulting oxidized molecule$^+$ is subsequently reduced by a suitable donor in solution (I^-) regenerating the molecule in its ground state.

The photocurrent responses measured at 0.3 V *vs.* Ag/AgCl for 3HF–TiO_2 and 3HF–Al_2O_3–TiO_2 photoelectrodes are reported in Fig. 9. The sample illuminated under chopped light shows a photocurrent overshoot at early times after the light-on transient and then decays to a rather stable photocurrent (on enlarging the illumination window) due to the oxidation of iodide to triiodide (I^- to I_3^-). To investigate the spectral dependence of the photo effect, long-pass filters of 455 nm and 495 nm were then applied. The photocurrent was markedly decreased when the filters were inserted and recovered their original value after the removal of the filters. Similar effects were observed for the 3HF–TiO_2 system and the 3HF–Al_2O_3–TiO_2 system (Fig. 7), with lower photocurrents in the latter case, as expected, due to the presence of the Al_2O_3 layer, which on the one hand physically hinders the charge injection and on the other hand favors a radiative charge decay through photoluminescence emission.

These results show that the photocurrent is sustained even by photons of wavelengths in the visible light, confirming that: (1) the photocurrent is due to injection from 3HF (the naked TiO_2 substrate does not generate photocurrents at these wave-

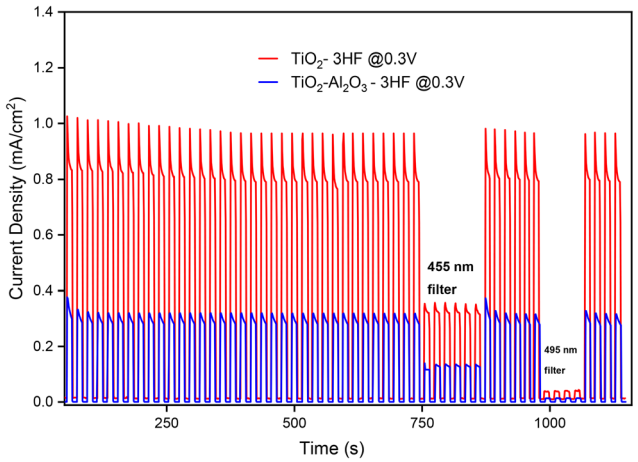

Fig. 9 Extended transient photocurrent responses of TiO_2–3HF and Al_2O_3–TiO_2–3HF (30 Å), at an applied potential of 0.3 V *vs.* Ag/AgCl. The photocurrent recorded under visible light illumination drops on inserting the long-pass filters at 455 nm and 495 nm and is fully recovered after their removal.

lengths, compared in Fig. S9†); and (2) photosensitization matches the spectrum of 3HF adsorbed on TiO_2 since the spectrum of the molecule in solution has no absorption for wavelengths higher than 400 nm in acidic medium (Fig. 2).

Electrochemical impedance spectroscopy (EIS) measurements showed that the charge transport resistance between the photoelectrode and the electrolyte is greatly affected by illumination, as shown by a comparison of the Nyquist plots recorded under different light conditions in Fig. S10 and S11 in the ESI†: (a) in the dark; (b) under full illumination by visible light; and (c) under visible light filtered using a long pass 455 nm filter. The EIS data were fitted using a simple Randles circuit provided in the inset of Fig. S10 in the ESI† and the fitting parameters are shown in Table S5 in the ESI.† For both photoelectrodes, under dark conditions, the charge transfer process was very difficult, as shown by the high values of the resistance (R_2 in Fig. S10a†), particularly in the case of the 3HF–Al_2O_3–TiO_2 system (Fig. S11 in the ESI†). However, the resistance values were substantially reduced under illumination by light absorbed by 3HF, confirming that the charge transfer across the interface is facilitated by a light-driven injection process.

We eventually performed transient transmission measurements through the pump–probe technique, tuning the pump photon energy at 400 nm, probing on a wide spectral range (~470–700 nm), detecting the differential transmission $\Delta T/T$ (where ΔT is the difference between the probe transmitted with and without pump excitation, see the Experimental section for details) at varying pump–probe delays. The data allowed us to access the dynamics of the generated charges immediately after photoexcitation, revealing crucial photophysical mechanisms. Fig. 8 reports the data for the 3HF loaded at nominal pH = 8, with and without the Al_2O_3 layer.

The transient transmission spectrum (inset of Fig. 10a) of TiO_2 NPs (red dashed line) was characterized by a broad negative signal, typical of this material,[51,52] corresponding to photoinduced absorption (PA) in the conduction band. It is noteworthy that, when 3HF is anchored directly on the metal oxide, the signal appears highly increased (thick dark blue line), while it is almost unchanged when the Al_2O_3 layer is present (thin light blue line). The higher signal observed clearly indicates that 3HF is injecting photogenerated charges into the conduction band of TiO_2, which is possible for direct anchoring. In Fig. 10, the PA dynamics are shown; the 3HF–TiO_2 sample (thick dark blue line) shows a very fast rise time of the signal, denoting an efficient charge transfer that takes place in less than 100 fs. Moreover, it is possible to observe that the signal is long lived (it appears flat for all the time delays that we could access, that is up to 1 ns), allowing us to exclude any backward transfer. Interestingly, the presence of the insulating layer (thin light blue line) led to a different scenario: the dynamics of the sample with and without 3HF appear very similar, with a small contribution due to charge injection. We further investigated the phenomenon by changing the pump fluence; the results are similar to the ones reported in Fig. 10a. In Fig. 10b, the signal evaluated at late time delays (around 4 ps) is plotted as a function of the pump fluence; this

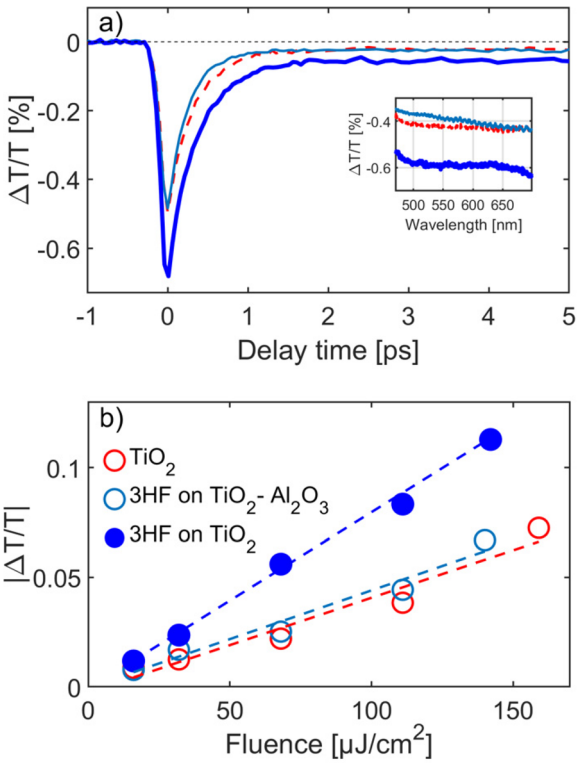

Fig. 10 Transient transmission $\Delta T/T$ data for 3HF (pH 8 uptake) anchored to the TiO_2 NP film with (thin light blue line) and without the 30 Å Al_2O_3 layer (thick dark blue line) and for the bare TiO_2 NP film (dashed red line). (a) Dynamics at a 605 nm probe wavelength, for a pump fluence of 70 μJ cm^{-2} (at the TiO_2 NP substrate); inset, corresponding spectra at 40 fs time delay; (b) $\Delta T/T$ absolute values, measured around 4 ps time delay, as a function of the pump fluence incident on TiO_2; dashed lines are linear and fits to experimental data.

signal accounts directly for the overall charges in TiO_2, available *e.g.* for the photocurrent. It should also be noted that 3HF directly anchored to TiO_2 resulted in a big increase, of about 90%, in available charges, compared to bare TiO_2, whereas the presence of the Al_2O_3 layer clearly reduces the injection, acting as a barrier. Similar results were found for the thicker insulation layer (100 Å Al_2O_3 layer) and with 3HF loaded at pH = 4, as reported in Fig. S12 in the ESI.†

It is noteworthy that these results were consistent with previous ones, in particular with the data on PL and photocurrent generation: as a matter of fact, charges photogenerated in the Ti–3HF complex are extracted by TiO_2, immediately after excitation, if no insulating layers are present, preventing any significant radiative decay in 3HF. In contrast, the presence of the Al_2O_3 layer, acting as a partial, but effective, barrier, allowed part of the photogenerated charges to remain in $[Al(3HF)_2]^+$ and undergo radiative recombination, resulting in the high PL of the surface complex, and the other part to be injected in TiO_2 and used for electrical current.

The results of photoelectrochemical and pump–probe experiments were consistent among themselves as well as with the outcomes obtained with the photoluminescent analyses and fit in a general scheme (Fig. S13 in the ESI†): (i) once 3HF is chemisorbed on the TiO_2 surface and irradiated, the surface complex is excited by visible light and is able to inject charges in the TiO_2 conduction band, generating a large anodic photocurrent; and (ii) the favorable energy alignment 3HF-TiO_2, *i.e.* the driving force leading to charge injection, is perturbed by the insertion of an insulating barrier (Al_2O_3), which lowers the photogenerated current and favors the alternative radiative decay of the metal complex, recorded as a large PL signal.

Conclusions

The present investigation reports a comprehensive, although preliminary, study on the photophysics of a representative flavonoid anchored on the surface of two metal oxides. This study may pave the way for new competitive optoelectronic materials characterized by easy fabrication and tunable properties, which can be used for a variety of applications, and suggests further research on the properties and potentialities of these materials.

3-Hydroxyflavone was successfully employed as a ligand to bind metal ions on the surface of a semiconducting and an insulating metal oxide, resulting in the formation of surface complexes.

The synthesis has an advantage of a very simple and fast procedure, producing a self-assembled monolayer of emitting species, whose decay to the ground state is either radiative or non-radiative depending on the nature of the metal oxide.

When 3HF is coordinated with aluminum ions on the Al_2O_3 surface, intense photoluminescence was observed, whose quantum yield of around 15% was quite high. On the other hand, the chelation of TiO_2 resulted in a system capable of simultaneous charge injection and light emission.

The properties of these systems strongly depend on the chemical nature of the coordinating metal ion, *i.e.* on the complex generated on the oxide surface, while the use of a semiconducting or insulating species can tune the decay fate of the photoexcited complexes, realizing a system preferably acting on design as a light emitter and an electron transport material.

The present investigation aimed at providing the proof of concept of the possibility of easily fabricating a potential optoelectronic material supporting two concomitant, competitive processes, namely light emission and charge transport. The possibilities enabled by this study are countless: indeed, by a proper coupling of a flavonoid moiety (whose family counts a huge amount of compounds featuring different and tunable characteristics) with a metal oxide (n- or p-type semiconductors as well as insulators), it would be possible to tune the optoelectronic properties, also accessing other phenomena like resonant charge transfer. Furthermore, the recently proposed theoretical possibility of engineering the band bending of a semiconductor by depositing an organic SAM on its surface[53] would represent an unexplored promising field of research in solid-state physics.

Conflicts of interest

There are no conflicts of interest.

References

1 S. V. Jovanovic, S. Steenken, M. Tosic, B. Marjanovic and M. G. Simic, Flavonoids as antioxidants, *J. Am. Chem. Soc.*, 1994, **116**, 4846–4851, DOI: **10.1021/ja00090a032**.
2 K. A. Youdim, B. Shukitt-Hale and J. A. Joseph, Flavonoids and the brain: Interactions at the blood–brain barrier and their physiological effects on the central nervous system, *Free Radicals Biol. Med.*, 2004, **37**, 1683–1693, DOI: **10.1016/j.freeradbiomed.2004.08.002**.
3 C. Rodríguez-García, C. Sánchez-Quesada, J. J. Gaforio and J. J. Gaforio, Dietary flavonoids as cancer chemopreventive agents: An updated review of human studies, *Antioxidants*, 2019, **8**, 1–23, DOI: **10.3390/antiox8050137**.
4 K. Pyrzynska and A. Pekal, Flavonoids as analytical reagents, *Crit. Rev. Anal. Chem.*, 2011, **41**, 335–345, DOI: **10.1080/10408347.2011.607077**.
5 S. Protti and A. Mezzetti, Any colour you like. Excited state and ground state proton transfer in flavonols and applications, *Photochemistry*, 2012, **40**, 295–322, DOI: **10.1039/9781849734882-29**.
6 M. Dendisová, D. Palounek, M. Švecová and V. Prokopec, SERS study of fluorescent and non-fluorescent flavonoids: What is the role of excitation wavelength on SERS optical response?, *Chem. Pap.*, 2019, **73**, 2945–2953, DOI: **10.1007/s11696-019-00757-2**.

7 M. Wang, T. Teslova, F. Xu, T. Spataru, J. R. Lombardi, R. L. Birke and M. Leona, Raman and surface enhanced Raman scattering of 3-hydroxyflavone, *J. Phys. Chem. C*, 2007, **111**, 3038–3043, DOI: **10.1021/jp062100i**.

8 E. Dündar, I. E. Mülazimoğlu and E. Özkan, . Electrochemical and spectroelectrochemical investigation of the behaviors of HF, 3-HF, 6-HF, 3,6-DHF on glassy carbon electrode surfaces, *Rev. Anal. Chem.*, 2011, **30**(1), 17–22, DOI: **10.1515/REVAC.2011.002**.

9 A. Landström, S. Leccese, H. Abadian, J. F. Lambert, I. Concina, S. Protti, A. P. Seitsonen and A. Mezzetti, Fluorescent Silica MCM-41 nanoparticles based on flavonoids: Direct post-doping encapsulation and spectral characterization, *Dyes Pigm.*, 2021, **185**, 108870, DOI: **10.1016/j.dyepig.2020.108870**.

10 S. Protti, K. Raulin, O. Cristini, C. Kinowski, S. Turrell and A. Mezzetti, Wavelength shifting systems based on flavonols and their metal complexes encapsulated by post-doping in porous SiO_2 xerogel matrices, *J. Mol. Struct.*, 2011, **993**, 485–490, DOI: **10.1016/j.molstruc.2011.02.010**.

11 S. Protti, A. Mezzetti, C. Lapouge and J. P. Cornard, Photochemistry of metal complexes of 3-hydroxyflavone: Towards a better understanding of the influence of solar light on the metal–soil organic matter interactions, *Photochem. Photobiol. Sci.*, 2007, **7**, 109–119, DOI: **10.1039/b709682h**.

12 M. M. Kasprzak, A. Erxleben and J. Ochocki, Properties and applications of flavonoid metal complexes, *RSC Adv.*, 2015, **5**, 45853–45877, DOI: **10.1039/c5ra05069c**.

13 M. Katyal, Flavones as analytical reagents – A review, *Talanta*, 1968, 95–106, DOI: **10.1016/0039-9140(68)80012-8**.

14 G. Alogero, J. H. Yum, A. Sinopoli, G. Di Marco, M. Grätzel and M. K. Nazeeruddin, Anthocyanins and betalains as light-harvesting pigments for dye-sensitized solar cells, *Sol. Energy*, 2012, **86**, 1563–1575, DOI: **10.1016/j.solener.2012.02.018**.

15 S. Shalini, R. Balasundara Prabhu, S. Prasanna, T. K. Mallick and S. Senthilarasu, Review on natural dye sensitized solar cells: Operation, materials and methods, *Renewable Sustainable Energy Rev.*, 2015, **51**, 1306–1325, DOI: **10.1016/j.rser.2015.07.052**.

16 G. Calogero, A. Bartolotta, G. Di Marco, A. Di Carlo and F. Bonaccorso, Vegetable-based dye-sensitized solar cells, *Chem. Soc. Rev.*, 2015, **44**, 3244–3294, DOI: **10.1039/c4cs00309h**.

17 G. Calogero, A. Sinopoli, I. Citro, G. Di Marco, V. Petrov, A. M. Diniz, A. J. Parola and F. Pina, Synthetic analogues of anthocyanins as sensitizers for dye-sensitized solar cells, *Photochem. Photobiol. Sci.*, 2013, **12**, 883–894, DOI: **10.1039/c3pp25347c**.

18 S. Sabagh, M. Izadyar and F. Arkan, Photovoltaic properties of the flavonoid-based photosensitizers: Molecular-scale perspective on the natural dye solar cells, *Int. J. Quantum Chem.*, 2020, **120**, 1–11, DOI: **10.1002/qua.26171**.

19 S. Çakar and M. Özacar, Fe-Quercetin coupled different shaped ZnO rods based dye sensitized solar cell applications, *Sol. Energy*, 2017, **155**, 233–245, DOI: **10.1016/j.solener.2017.06.017**.

20 M. A. Dil, A. Haghighatzadeh and B. Mazinani, Photosensitization effect on visible-light-induced photocatalytic performance of TiO_2/chlorophyll and flavonoid nanostructures: Kinetic and isotherm studies, *Bull. Mater. Sci.*, 2019, **42**, 1–16, DOI: **10.1007/s12034-019-1927-9**.

21 A. Zdyb and S. Krawczyk, Adsorption and electronic states of morin on TiO_2 nanoparticles, *Chem. Phys.*, 2014, **443**, 61–66, DOI: **10.1016/j.chemphys.2014.08.009**.

22 Q. Zhou, H. Zhang, Y. Wang and X. Zhou, Studies on the interaction of interface between morin and TiO_2, *Spectrochim. Acta, Part A*, 2009, **72**(1), 110–114, DOI: **10.1016/j.saa.2008.08.012**.

23 P. Chinwangso, A. C. Jamison and T. R. Lee, Multidentate adsorbates for self-assembled monolayer films, *Acc. Chem. Res.*, 2011, **44**, 511–519, DOI: **10.1021/ar200020s**.

24 S. Casalini, C. A. Bortolotti, F. Leonardi and F. Biscarini, Self-assembled monolayers in organic electronics, *Chem. Soc. Rev.*, 2017, **46**, 40–71, DOI: **10.1039/c6cs00509h**.

25 C. Prasittichai, J. R. Avila, O. K. Farha and J. T. Hupp, Systematic modulation of quantum (electron) tunneling behavior by atomic layer deposition on nanoparticulate SnO_2 and TiO_2 photoanodes, *J. Am. Chem. Soc.*, 2013, **135**, 16328–16331, DOI: **10.1021/ja4089555**.

26 L. J. Antila, M. J. Heikkilä, V. Mäkinen, N. Humalamäki, N. Laitinen, V. Linko, P. Jalkanen, J. Toppari, V. Aumanen, M. Kemell, P. Myllyperkiö, K. Honkala, H. Häkkinen, M. Leskelä and J. E. I. Korppi-Tommola, ALD grown aluminum oxide submonolayers in dye-sensitized solar cells: The effect on interfacial electron transfer and performance, *J. Phys. Chem. C*, 2011, **115**, 16720–16729, DOI: **10.1021/jp204886n**.

27 E. Palomares, J. N. Clifford, S. A. Haque, T. Lutz and J. R. Durrant, Control of charge recombination dynamics in dye sensitized solar cells by the use of conformally deposited metal oxide blocking layers, *J. Am. Chem. Soc.*, 2003, **125**, 475–482, DOI: **10.1021/ja027945w**.

28 K. Hanson, M. D. Losego, B. Kalanyan, G. N. Parsons and T. J. Meyer, Stabilizing small molecules on metal oxide surfaces using atomic layer deposition, *Nano Lett.*, 2013, **13**, 4802–4809, DOI: **10.1021/nl402416s**.

29 K. Hanson, M. D. Losego, B. Kalanyan, D. L. Ashford, G. N. Parsons and T. J. Meyer, Stabilization of $[Ru(Bpy)_2(4,4'\text{-}(PO_3H_2)Bpy)]^{2+}$ on mesoporous TiO_2 with atomic layer deposition of Al_2O_3, *Chem. Mater.*, 2013, **25**, 3–5, DOI: **10.1021/cm303172w**.

30 D. Calestani, Characterization of the physical and chemical properties of engineered nanomaterials, in *Exposure to Engineered Nanomaterials in the Environment*, ed. N. Marmiroli, J. C. White and J. Song, Elsevier, 2019, pp. 31–57. DOI: **10.1016/C2017-0-01491-X**.

31 W. Macyk, K. Szaciłowski, G. Stochel, M. Buchalska, J. Kuncewicz and P. Łabuz, Titanium(IV) complexes as direct TiO_2 photosensitizers, *Coord. Chem. Rev.*, 2010, **254**, 2687–2701, DOI: **10.1016/j.ccr.2009.12.037**.

32 M. Gilzad Kohan, A. Vomiero, S. You, A. Camellini, I. Concina and M. Zavelani-Rossi, Optical field coupling in ZnO nanorods decorated with silver plasmonic nanoparticles, *J. Mater. Chem. C*, 2021, **9**, 15452–15462, DOI: **10.1039/d1tc03032a**.

33 P. K. Mandal and A. Samanta, . Evidence of ground-state proton-transfer reaction of 3-hydroxyflavone in neutral alcoholic solvents, *J. Phys. Chem. A*, 2003, **107**, 6334–6339, DOI: **10.1021/jp027613d**.

34 I. Concina, E. Frison, A. Braga, S. Silvestrini, M. Maggini, G. Sberveglieri, A. Vomiero and T. Carofiglio, On-line monitoring and active control of dye uptake in dye-sensitised solar cells, *Chem. Commun.*, 2011, **47**, 11656–11658, DOI: **10.1039/c1cc14571a**.

35 E. Dell'Orto, L. Raimondo, A. Sassella and A. Abbotto, Dye-sensitized solar cells: Spectroscopic evaluation of dye loading on TiO_2, *J. Mater. Chem.*, 2012, **22**, 11364–11369, DOI: **10.1039/c2jm30481c**.

36 D. McMorrow and M. Kasha, Proton-transfer spectroscopy of 3-hydroxyflavone in an isolated-site crystal matrix, *Proc. Natl. Acad. Sci. U. S. A.*, 1984, **81**, 3375–3378, DOI: **10.1073/pnas.81.11.3375**.

37 S. Lazzaroni, D. Dondi, A. Mezzetti and S. Protti, Role of solute-solvent hydrogen bonds on the ground state and the excited state proton transfer in 3-hydroxyflavone. A systematic spectrophotometric study, *Photochem. Photobiol. Sci.*, 2018, **17**, 923–933, DOI: **10.1039/c8pp00053k**.

38 K. Zhu, T. Lv, T. Qin, Y. Huang, L. Wang and B. Liu, A flavonoid-based fluorescent probe enables the accurate quantification of human serum albumin by minimizing the interference from blood lipids, *Chem. Commun.*, 2019, **55**, 13983–13986, DOI: **10.1039/c9cc08015e**.

39 A. P. Seitsonen, A. Idrissi, S. Protti and A. Mezzetti, Solvent effects on the vibrational spectrum of 3-hydroxyflavone, *J. Mol. Liq.*, 2019, **275**, 723–728, DOI: **10.1016/j.molliq.2018.11.020**.

40 Y. A. Davila, M. I. Sancho, M. C. Almandoz and S. E. Blanco, Structural and spectroscopic study of Al(III)-3-hydroxyflavone complex: Determination of the stability constants in water–methanol mixtures, *Spectrochim. Acta, Part A*, 2012, **95**, 1–7, DOI: **10.1016/j.saa.2012.04.034**.

41 A.-C. Boudet, J.-P. Cornard and J.-C. Merlin, Conformational and spectroscopic investigation of 3-hydroxyflavone–aluminium chelates, *Spectrochim. Acta, Part A*, 2000, **56**, 829–839, DOI: **10.1016/S1386-1425(99)00284-X**.

42 K. Tennakone, G. R. R. A. Kumara, A. R. Kumarasinghe, P. M. Sirimanne and K. G. U. Wijayantha, Efficient photosensitization of nanocrystalline TiO_2 films by tannins and related phenolic substances, *J. Photochem. Photobiol., A*, 1996, **94**, 217–220, DOI: **10.1016/1010-6030(95)04222-9**.

43 G. Gheno, N. R. De Souza Basso, M. A. Ceschi, P. R. Livotto, A. A. Nascimento, Z. N. Da Rocha and G. B. Galland, Flavone complexes of Ti and Zr active in ethylene polymerization, *Appl. Catal., A*, 2013, **467**, 439–449, DOI: **10.1016/j.apcata.2013.08.015**.

44 F. A. Cotton and G. Wilkinson, *Advanced Inorganic Chemistry A Comprehensive Text*, 4th edn, John Wiley & Sons, New York, 1980.

45 R. Breslow, The Chelate Effect in Binding, Catalysis, and Chemotherapy, *Recl. Trav. Chim. Pays-Bas*, 1994, **113**, 493–498, DOI: **10.1002/recl.19941131102**.

46 E. I. Davydova, T. N. Sevastianova, A. Y. Timoshkin, A. V. Suvorov and G. Frenking, Chelate effect: The importance of reorganization energy, *Int. J. Quantum Chem.*, 2004, **100**, 419–425, DOI: **10.1002/qua.20094**.

47 A. D. Baker and R. Engel, *Organic Chemistry*, West Group, 1992.

48 S. Cattarin, P. Ceroni, D. M. Guldi, M. Maggini, E. Menna, F. Paolucci, S. Roffia and G. Scorrano, Synthesis and photoelectrochemical properties of a fullerene–azothiophene dyad, *J. Mater. Chem.*, 1999, **9**, 2743–2750, DOI: **10.1039/a905287i**.

49 M. L. Foresti, S. Milani, F. Loglio, M. Innocenti, G. Pezzatini and S. Cattarin, Ternary CdS_xSe_{1-x} Deposited on Ag(111) by ECALE: Synthesis and characterization, *Langmuir*, 2005, **21**, 6900–6907, DOI: **10.1021/la050176k**.

50 R. Milan, S. Cattarin, N. Comisso, C. Baratto, K. Kaunisto, N. V. Tkachenko and I. Concina, Compact hematite buffer layer as a promoter of nanorod photoanode performances, *Sci. Rep.*, 2016, **6**, 1–27, DOI: **10.1038/srep35049**.

51 I. Concina, C. Manzoni, G. Grancini, M. Celikin, A. Soudi, F. Rosei, M. Zavelani-Rossi, G. Cerullo and A. Vomiero, Modulating exciton dynamics in composite nanocrystals for excitonic solar cells, *J. Phys. Chem. Lett.*, 2015, **6**, 2489–2495, DOI: **10.1021/acs.jpclett.5b00765**.

52 Y. Yang, W. Rodríguez-Córdoba, X. Xiang and T. Lian, Strong electronic coupling and ultrafast electron transfer between PbS quantum dots and TiO_2 nanocrystalline films, *Nano Lett.*, 2012, **12**, 303–309, DOI: **10.1021/nl2035783**.

53 O. T. Hofmann and P. Rinke, Band bending engineering at organic/inorganic interfaces using organic self-assembled monolayers, *Adv. Electron. Mater.*, 2017, **3**, 1600373, DOI: **10.1002/aelm.201600373**.